

Supplementary information to: “Probing single-charge fluctuations at a GaAs/AlAs interface using laser spectroscopy on a nearby InGaAs quantum dot”

J. Houel, A. Kuhlmann, L. Greuter, F. Xue, M. Poggio, and R. J. Warburton
Department of Physics, University of Basel, Klingelbergstrasse 82, CH-4056 Basel, Switzerland

B. D. Gerardot and P. A. Dalgarno
School of Engineering and Physical Sciences, Heriot-Watt University, Edinburgh EH14 4AS, UK

A. Badolato
Department of Physics and Astronomy, University of Rochester, Rochester, New York 14627, USA

P. M. Petroff
Materials Department, University of California, Santa Barbara, California 93106, USA

A. Ludwig, D. Reuter, and A. D. Wieck
Lehrstuhl für Angewandte Festkörperphysik, Ruhr-Universität Bochum, D-44780 Bochum, Germany

In “Probing single-charge fluctuations at a GaAs/AlAs interface using laser spectroscopy on a nearby InGaAs quantum dot” [1], a single quantum dot (QD) is used as a nano-sensor of its own local electrical environment. The understanding of the local electrical fluctuations has led to a new sample design where close-to-transform-limited linewidths are routinely measured. These conclusions rely on experimental results which we model with Monte-Carlo simulations. The details of these simulations are explained in this supplementary information. We explain how the input parameters are determined and how the results depend on the defect density, defect positions and occupation probabilities.

PACS numbers: 73.21.La and 78.67.Hc

PART I: MONTE-CARLO SIMULATION OF THE CHARGE FLUCTUATIONS: CALCULATION

1. Stark shift

The interpretation of the experiments relies on the DC-Stark effect of the single negatively charged exciton, X^{1-} . The dependence of the X^{1-} emission energy as a function of an external electric field \mathbf{F}_0 is given by [2]:

$$E_{X^{1-}}^{(1)} = E_0 + \sum_{i=x,y,z} (-p_i F_{0,i} + \beta_i F_{0,i}^2) \quad (1)$$

where p_i , β_i and $F_{0,i}$ are the permanent dipole moment, the polarizability and the bare electric field in direction i , respectively. The emission energy with an additional electric field \mathbf{F}_h is similarly given by:

$$E_{X^{1-}}^{(2)} = E_0 + \sum_{i=x,y,z} (-p_i (F_{0,i} + F_{h,i}) + \beta_i (F_{0,i} + F_{h,i})^2). \quad (2)$$

The energy shift ΔE induced by the additional electric field \mathbf{F}_h is then given by $E_{X^{1-}}^{(2)} - E_{X^{1-}}^{(1)}$:

$$\Delta E = \sum_{i=x,y,z} (-p_i F_{h,i} + \beta_i F_{h,i} (F_{h,i} + 2F_{0,i})). \quad (3)$$

2. Electric field created by a single hole

We consider a single positive charge located at distance d_{cap} from the QD in the growth direction (z), at lateral coordinate $\mathbf{r} = (x, y) = (r, \theta)$ with the dot at $\mathbf{r} = 0$, Fig. 1. The back contact is treated as a metallic layer, implying the creation of a negative image charge. The resulting potential is then given by:

$$V_h(x, y, z) = \frac{e}{4\pi\epsilon_0\epsilon_r} \left[\frac{1}{\sqrt{(\delta - z)^2 + x^2 + y^2}} - \frac{1}{\sqrt{(\delta + z)^2 + x^2 + y^2}} \right]. \quad (4)$$

The electric field created by this single charge is deduced from $\mathbf{F}_h = -\nabla V_h$:

$$\begin{aligned} F_{h,x}(x, y, z) &= + \frac{ex}{4\pi\epsilon_0\epsilon_r} \left[\frac{1}{((\delta - z)^2 + x^2 + y^2)^{\frac{3}{2}}} - \frac{1}{((\delta + z)^2 + x^2 + y^2)^{\frac{3}{2}}} \right], \\ F_{h,y}(x, y, z) &= + \frac{ey}{4\pi\epsilon_0\epsilon_r} \left[\frac{1}{((\delta - z)^2 + x^2 + y^2)^{\frac{3}{2}}} - \frac{1}{((\delta + z)^2 + x^2 + y^2)^{\frac{3}{2}}} \right], \\ F_{h,z}(x, y, z) &= - \frac{e}{4\pi\epsilon_0\epsilon_r} \left[\frac{\delta - z}{((\delta - z)^2 + x^2 + y^2)^{\frac{3}{2}}} + \frac{\delta + z}{((\delta + z)^2 + x^2 + y^2)^{\frac{3}{2}}} \right]. \end{aligned} \quad (5)$$

The electric field at the location of the QD is given by eq. 5 with $z = d_{\text{tun}}$.

3. Stark shift parameters in the growth direction

In the growth direction, the dipole moment and polarizability, p_z and β_z , are determined by fitting the voltage dependence of the X^{1-} photoluminescence (PL) emission spectrum [2]. The non-resonant laser in PL experiments creates stored holes at the capping layer/short period superlattice (SPS) interface, a space charge, shifting the charging plateaux in gate voltage. In this case, $F_{0,z}$ is given by:

$$F_{0,z} = \frac{V_0 - V_g}{D} + \Delta F_{\text{NR}} \quad (6)$$

where V_g , V_0 and D are the applied gate voltage, the Schottky barrier of the gate, and the back contact to surface distance, respectively. ΔF_{NR} is the additional electric field arising from the space charge. ΔF_{NR} is determined by insisting that the local absorption shift measured with resonant laser spectroscopy, $765 \mu\text{eV/V}$ for the QD of sample A [1], is reproduced. For this particular QD, the fixed parameters are $D = 175 \text{ nm}$, $V_g = -0.05 \text{ V}$ and $V_0 = 0.62 \text{ V}$. From the fit, we obtain:

$$\begin{aligned} p_z &= -0.231 \text{ nm} \\ \beta_z &= -0.386 \mu\text{eV}/(\text{kV}/\text{cm})^2 \\ \Delta F_{\text{NR}} &= 9.0 \text{ kV}/\text{cm}. \end{aligned} \quad (7)$$

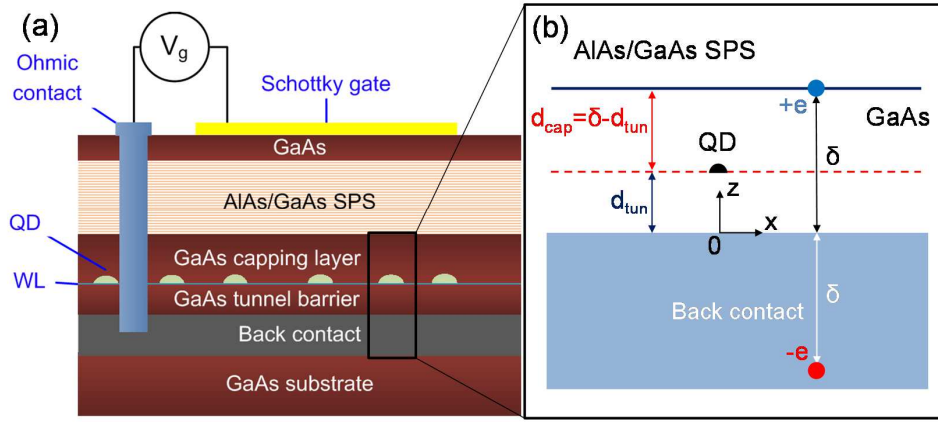


FIG. 1. (a) Structure of the samples. The active layer consists of a layer of quantum dots (QDs), a GaAs tunnel barrier below the QDs and a GaAs capping layer above. An AlAs/GaAs short period superlattice (SPS) is grown on top of the capping layer. The Schottky gate is a semi-transparent metal layer deposited on the sample surface. Ohmic contacts are prepared to the back contact. (b) Zoom-in of the active region in (a). A QD is separated from the capping layer/SPS interface by distance d_{cap} and from the back contact by distance d_{tun} . A single hole is shown at the capping layer/SPS interface at $z = \delta$, creating a negative image charge at $z = -\delta$.

4. Stark shift parameters in the QD plane

The in-plane permanent dipole moments p_x and p_y are assumed to be zero [3]. Assuming a harmonic confining potential, the polarizability in the QD plane is given by [2]:

$$\beta_x = \beta_y = -e^2 \frac{m_e l_e^4 + m_h l_h^4}{2\hbar^2} \quad (8)$$

where $m_e = 0.07m_0$ and $m_h = 0.25m_0$ are the electron and hole in-plane effective masses, and l_e and l_h are the lateral extents of the electron and hole wave functions, respectively [4]. The parameters l_e and l_h can be determined from the PL charging diagram [4]; specifically, from the extent of the neutral exciton charging plateau $\Delta V(X^0)$ and from the PL energy difference between X^{1-} and X^0 , $\Delta E_{\text{PL}}(X^{1-} - X^0)$ [5]. l_e can be expressed as a function of the electron-electron interaction energy in the ground state E_{ee}^{ss} :

$$l_e = \frac{e^2}{4\pi\epsilon_0\epsilon_r} \sqrt{\frac{\pi}{2}} \frac{1}{E_{ee}^{\text{ss}}}, \quad (9)$$

with [4]:

$$E_{ee}^{\text{ss}} = \frac{\Delta V(X^0)}{\lambda} - 2E_j \quad (10)$$

where λ is the sample lever arm and E_j the Coulomb energy of an electron in the QD with its image charge in the back contact ($E_j = 1.1$ meV for $d_{\text{tun}} = 25$ nm). Once l_e is known, l_h can be determined from the electron-hole Coulomb energy:

$$E_{eh}^{\text{ss}} = \frac{e^2\sqrt{\pi}}{4\pi\epsilon_0\epsilon_r} \frac{1}{\sqrt{l_e^2 + l_h^2}} = E_{ee}^{\text{ss}} - \Delta E_{\text{PL}}(X^{1-} - X^0). \quad (11)$$

This gives $l_e = 4.24$ nm and $l_h = 2.45$ nm for the QD from sample A in [1], leading to $\beta_x = \beta_y = -2.06 \mu\text{eV}/(\text{kV}/\text{cm})^2$. Finally, as the applied electric field is in the growth direction, we take $F_{0,x} = F_{0,y} = 0$.

5. Stark shifts: growth direction versus in-plane fields

With the parameters obtained above for the QD in sample A, we compare the contributions of electric fields and Stark shifts generated in the growth and in-plane directions for $d_{\text{cap}} = 30$ nm and $d_{\text{tun}} = 25$ nm. As a typical case, we consider a single hole trapped at the capping layer/SPS interface with in-plane coordinates $(x, y) = (10, 0)$ nm. We obtain:

$$F_z = -1.29 \text{ kV}/\text{cm}$$

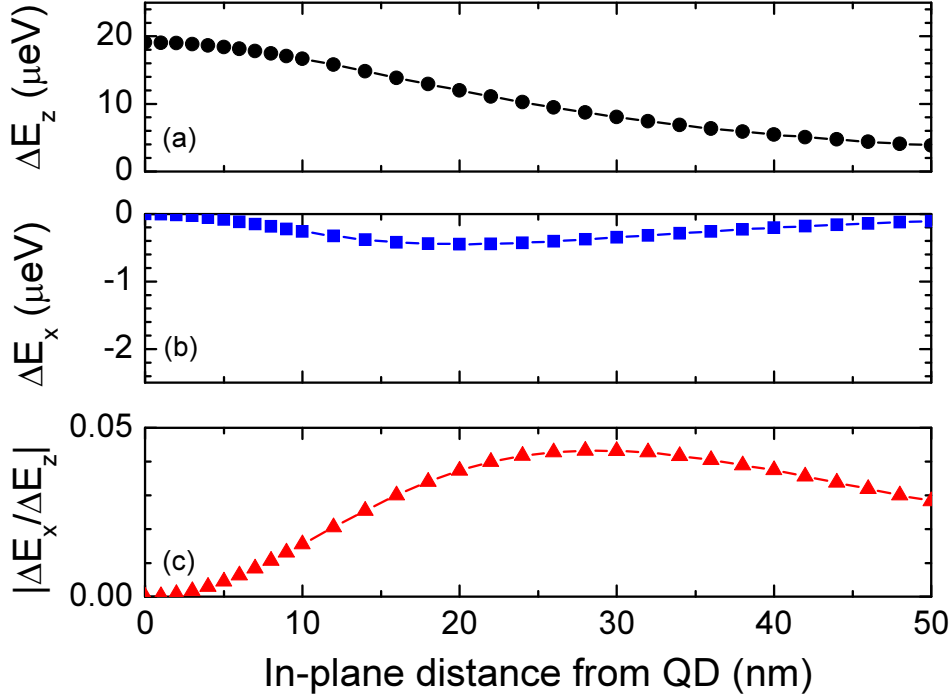


FIG. 2. (a) ΔE_z and (b) ΔE_x as a function of the in-plane defect distance from the QD, calculated using the parameters from section I.3 and I.4. (c) Ratio $|\Delta E_x/\Delta E_z|$ as a function of the in-plane defect distance from the QD. The in-plane Stark shift is always more than one order of magnitude smaller than the Stark shift in the growth direction. The largest ratio is $|\Delta E_x/\Delta E_z| \approx 4\%$.

$$\begin{aligned}
 F_x &= -0.35 \text{ kV/cm} \\
 F_y &= 0 \\
 \Delta E_z &= 16.7 \text{ } \mu\text{eV} \\
 \Delta E_x &= -0.26 \text{ } \mu\text{eV} \\
 \Delta E_y &= 0.
 \end{aligned} \tag{12}$$

We observe that the effect of the in-plane component is two orders of magnitude smaller than that in the growth direction. We generalize this comparison in Fig. 2 where ΔE_z , ΔE_x and the ratio $|\Delta E_x/\Delta E_z|$ are plotted as a function of the in-plane defect location, showing that for all x , $|\Delta E_x| \ll |\Delta E_z|$.

6. The Monte-Carlo population of the defects with holes

An array of defects is considered at the capping layer/SPS interface. The defects are populated randomly in a Monte-Carlo simulation. Defect i is populated with a weighted probability $\alpha_i p$, where p is the control parameter of the simulations, $0 \leq p \leq 1$. $\alpha_i p$ rises with p until it reaches 100%; at larger values of p , the probability is clamped to 100%. The α -parameter can change from defect to defect and represents, at a particular p , the relative probability of occupying a particular localization center. Its value is $\alpha_i \geq 1$ for all i to ensure that all the defects are populated at $p = 1$.

A defect array is defined, specifying for each defect the location (x_i, y_i) and the weighting factor α_i . A value of p is then chosen. Each defect is “tested” with respect to a random number g , $0 \leq g \leq 1$. If $\alpha_i p > g$, defect i is populated with one hole. If $\alpha_i p \leq g$, defect i is not populated. This process is repeated for each defect, generating a new random number g for each defect. In this way, a distribution of localized charges at the capping layer/SPS interface is created. The electric field at the location of the quantum dot arising from the localized holes is calculated by adding up the electric field from each localized charge (repeated use of eq. 5). The Stark shift of the optical transition is then calculated with eq. 3. These successive steps consider one and only one particular charge distribution at the interface. In order to reproduce the experiments, we run this procedure N times. From one run to the next, the spatial distribution of the defects remains the same, as does the control variable p , but otherwise the runs are not correlated with each other. The final optical spectrum is a sum over N runs. The entire process is then repeated as a

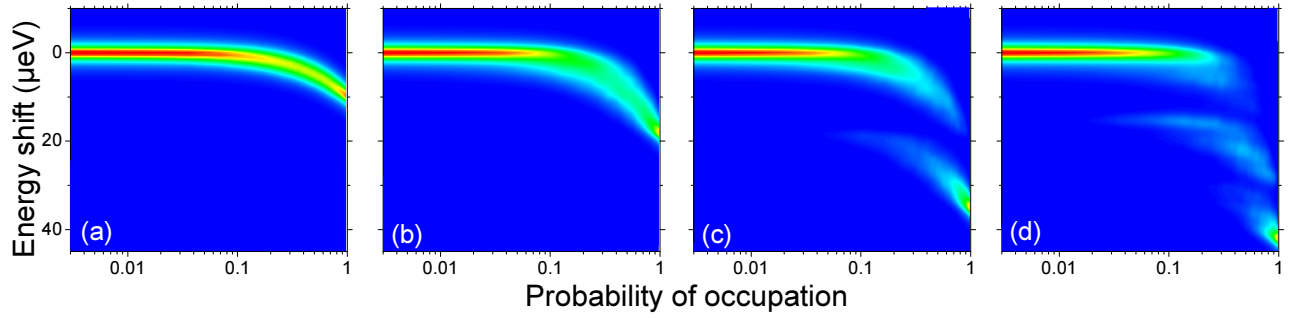


FIG. 3. (a)-(d) Example simulations obtained with a 2D random distribution of defects with $N_{2D} = 10^{10} \text{ cm}^{-2}$ over a surface of $1.0 \mu\text{m}^2$. The parameters are the ones obtained for the QD in sample A in section I with $N = 2,500$ and $\Gamma_L = 1.0 \mu\text{m}$. The color scale goes from 2 (blue) to 60 (red). More than 50% of the simulated contour plots are similar to (a) and (b); some show steps, (c) and (d).

function of p .

7. Spatial modulation of the probability of occupation

In order to include the Gaussian beam profile of the non-resonant excitation, the weighting factors α_i are multiplied by a normalized Gaussian function, the Gaussian a function of r_i , centered on the QD, with a full width at half maximum (FWHM) Γ_L .

8. Exciton inhomogeneous broadening

The exciton spectrum is broadened, in general with homogeneous and inhomogeneous components. Each discrete energy shift obtained in the simulation is replaced with a normalized Lorentzian with full-width-at-half-maximum Γ . For sample A, we take $\Gamma = 2.5 \mu\text{eV}$, an inhomogeneous broadening. For samples B and C, we take $\Gamma = 0.8 \mu\text{eV}$ corresponding to homogeneous broadening, equivalently the radiative lifetime-limited linewidth, the so-called “transform limit”.

PART II: MONTE-CARLO SIMULATION OF THE CHARGE FLUCTUATIONS: RESULTS

1. The defect array

We present initially simulation results obtained with $d_{\text{tun}} = 25 \text{ nm}$, $d_{\text{cap}} = 30 \text{ nm}$, corresponding to samples A and B, using a full 2D array of randomly placed defects with density N_{2D} . Fig. 3 shows example simulation results, energy shift versus p , from a set of 500 runs using the Stark shift parameters for the QD in sample A and with $N_{2D} = 1 \times 10^{10} \text{ cm}^{-2}$. We find that, first, a large percentage of the simulated contour plots show a monotonous Stark shift as a function of p without any steps (56.8 %; 284 occurrences in the 500 Monte Carlo simulations). Two typical examples are shown in Fig. 3(a),(b). Some other simulations exhibit clearly-resolved steps in the Stark shift versus p plots, Fig. 3(c),(d). In this simulation set, only 1 of the 500 runs exhibits 5 steps, a probability of $\sim 0.2\%$. The probability of 4 steps is $\sim 0.4\%$; the probability of 3 steps 4.2%. The probability of steps occurring is even smaller for a lower value of N_{2D} . At higher values of N_{2D} , steps are more likely, but the transition from one step to the other becomes progressively more blurred such that above $6 \times 10^{10} \text{ cm}^{-2}$, no well defined steps can be made out. Another significant point is that when steps are observed, for instance Fig. 3(c),(d), the absorption energy within each “plateau” has a strong dependence on p , shifting monotonically to the blue.

These results are now tensioned against the experiments. For all 8 quantum dots measured with $d_{\text{cap}} = 30 \text{ nm}$, all 8 exhibit steps in the absorption versus non-resonant laser power (P) plots. Example data are shown in Fig. 2(a) of [1] (sample A), and Fig. 4(a) (sample B). All the dots show at least 3 steps. One dot shows 6 steps with a total Stark shift of $\sim 300 \mu\text{eV}$, a situation we have not encountered even in several thousand simulations using a homogeneous N_{2D} . The conclusion is that there are localization centers located directly above the quantum dot which are highly unlikely to arise by a process which is completely random as a function of (x, y) . Instead, the quantum dot induces localization centers at the capping layer/SPS interface for

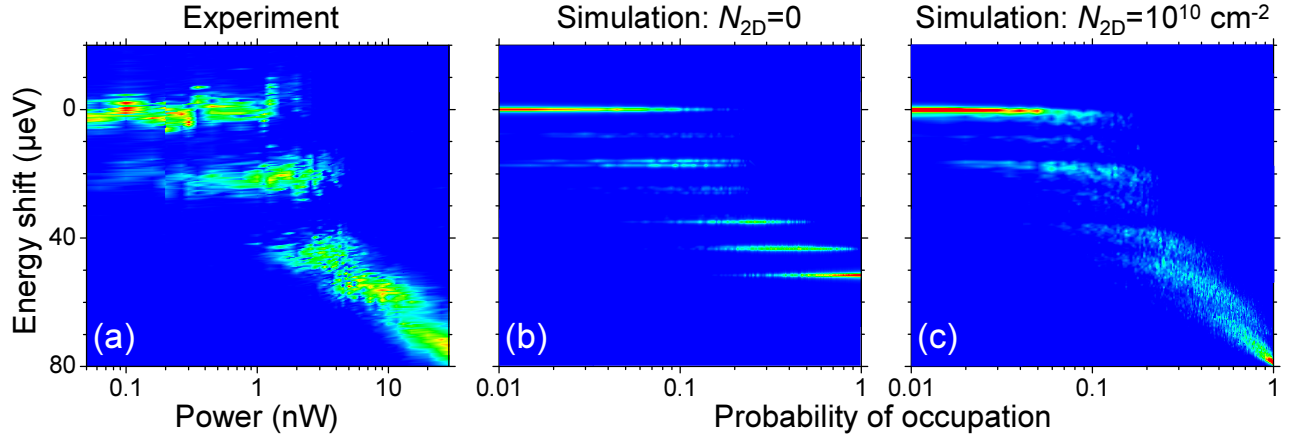


FIG. 4. (a) Contour plot of the QD resonance fluorescence signal from sample B as a function of the non-resonant excitation power. The color scale goes from 27 counts (blue) to 700 counts (red). (b),(c) Simulated signal as a function of the probability of occupation, plotted with the same scale dynamic as (a), i.e. 0.15 (blue) to 4 (red). (b) $N_{2D} = 0$; (c) $N_{2D} = 1.0 \times 10^{10} \text{ cm}^{-2}$. An area of $3 \times 3 \mu\text{m}^2$ is considered; $\Gamma_L = 10.0 \mu\text{m}$, $N = 60$ and $\Gamma = 0.8 \mu\text{eV}$. From the PL characterization, $V_g = -0.7 \text{ V}$, $V_0 = 0.62 \text{ V}$, $D = 322 \text{ nm}$, $p_z = 0.142 \text{ nm}$, $\beta_z = -0.104 \mu\text{eV}/(\text{kV}/\text{cm})^2$, $\Delta F_{\text{NR}} = 13 \text{ kV}/\text{cm}$, $l_e = 5.02 \text{ nm}$ and $l_h = 2.88 \text{ nm}$. In addition to N_{2D} , 4 defects were placed by hand to reproduce the energy steps, with in-plane positions $r_i = (28, 45, 45, 26) \text{ nm}$ and $\alpha = (4.0, 1.7, 1.0, 4.0)$.

$d_{\text{cap}} = 30 \text{ nm}$, typically two to four, the “above-dot-defects”. Occupation of these defects leads to the pronounced steps in the Stark shift versus P experimental results, equivalently the Stark shift versus p simulations.

For the QD in sample A, the P -dependence of each Stark shift “plateau” is small, Fig. 2(a) of [1]. As explained above, this signifies that N_{2D} is small. In fact, N_{2D} is too small for us to resolve and we take $N_{2D} = 0$ in the simulations, Fig. 2(b) of [1] and Fig. 5. However, QDs in sample B behave differently, Fig. 4(a). In this case, the plateau steps show a blue shift, particularly when the defects directly above the quantum dot (4 in this case), are occupied (by 3 – 4 holes in this case). In addition, each absorption line in the experiment changes from run to run, the origin of the noise in Fig. 4(a). Neither the blue shifts nor the noise can be reproduced in the simulations with $N_{2D} = 0$ as shown in Fig. 4(b). Instead, $N_{2D} \neq 0$. For a given occupation of the defects directly above the dot, as p increases, the number of stored holes at the capping layer/SPS interface increases, inducing the blue shifts of the plateau. Also, for fixed p , changes in the charge distribution of the holes leads to small energy shifts even when the number of holes in the above-dot-defects remains constant, leading to the noise. For a quantum dot in sample B, we fix the positions of the above-dot-defects using the procedure outlined below, we define a random 2D array for $r \geq 80 \text{ nm}$, and then vary N_{2D} to find the best fit to the experimental data: $N_{2D} = 1 \times 10^{10} \text{ cm}^{-2}$ gives good agreement with the experimental results, Fig. 4(c).

2. Positions of above-dot-defects

We illustrate how the simulation can enable us to deduce the positions of the above-dot-defects, concentrating on the results from sample A, Fig. 2(a) in [1]. (Fig. 4 illustrates the result of the same procedure on a dot from sample B.) Fig. 5 shows different contour plots obtained by changing the properties of the above-dot-defects, illustrating the procedure for reaching the best fit for QD in sample A, Fig. 2(b) in [1]. The number of steps, 4 in this case, determines the total number of holes which can be stored in the above-dot-defects. In Fig. 5(a), 4 defects are placed at the same location, all with the same weight $\alpha = 1$, laterally displaced from the quantum dot in order to reproduce the total Stark shift in the experiment. Four steps and 5 transitions are simulated, as in the experiment. The “size” of the steps decreases slightly with increasing hole number – the in-plane Stark shift increases in magnitude and subtracts from the vertical Stark shift – but this does not match the experimental result, Fig. 2 [1]. In Fig. 5(b), the defects are now placed one in each quadrant around the QD, keeping $r = \sqrt{x^2 + y^2}$ constant. Now, the step sizes are constant – the in-plane electric fields tend to cancel – in slightly better but still poor agreement with the experimental result. The markedly different step sizes in the experiment can be reproduced in the simulation only by changing both the locations of the defects r_i and their relative weights α_i . In Fig. 5(c), the 4 defects are located at 4 different values of r . The Stark shift versus p plot is now more complicated. For instance, while 2 stored holes in Fig. 5(b) give the same Stark shift independent of the configuration, this is no longer the case in Fig. 5(c): the 4-fold degeneracy is lifted. Line cuts show that Fig. 5(c) has transitions at the correct energies but the relative transition strengths are not reproduced. This discrepancy is remedied by changing the α_i . The result of this procedure is shown in Fig. 5(h). A defect with relatively large r has a particularly large α : this produces a

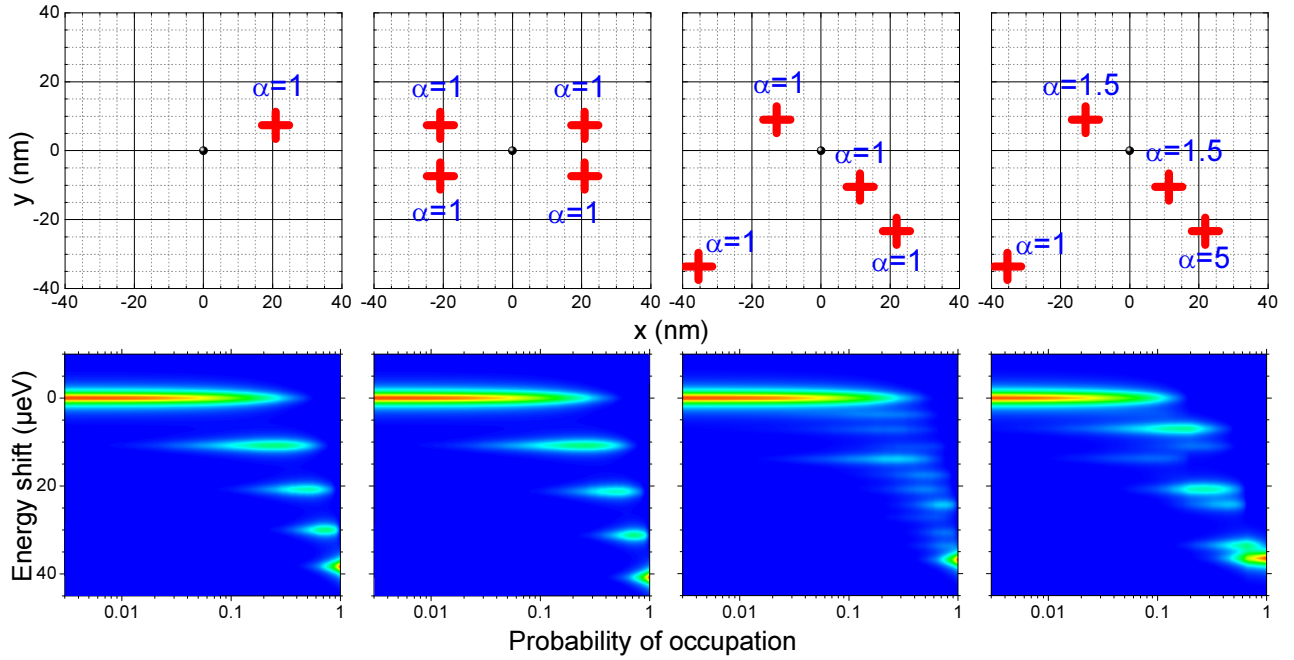


FIG. 5. (a)-(d) 2D representation of the spatial distribution of defects used in the simulations (e)-(h). The QD is symbolized by the black disk in the center of each 2D map. In (a), all the 4 defects are located at the same place with $r = 22.1$ nm. In (b), r is kept constant, only θ is changed. In (c) and (d), the spatial distribution is the one used in [1]. The weight α associated to each defect is specified explicitly. The color scale goes from 4 (blue) to 135 (red). $N_{2D} = 0$. The parameters used for the simulations are those for the QD in sample A [1], described in section I, with $N = 2,500$ and $\Gamma_L = 1.0 \mu\text{m}$.

small first step. Once this defect is always occupied, $p > 0.2$, occupation of the remaining 3 gives the remaining step structure in close agreement with the experiment.

3. Spatial resolution of the defect positions

A quantitative agreement with the peak positions and relative amplitudes in the experiment, Fig. 2 of [1], can only be achieved with a tolerance of ± 5 nm in each of the r_i values. This spatial resolution is illustrated in Fig. 6, where we move, from the ideal distribution, the different defects within 5 nm and examine the peak positions in both the experiments and simulations, Fig. 6, for a particular value of P , equivalently p . Fig. 6(a),(g) represent the best fit to the data. Fig. 6(b),(h) show results for a distribution where all the defects have been moved 5 nm towards the QD. The two main peaks in the simulations are now blue shifted with respect to the experiment at this particular p ; also, the simulated Stark shift at $p = 1$ is also too large. Fig. 6(c),(e) and (i),(k) show results when only one of the defects is moved by plus or minus 5 nm. One can see that there is always at least one energy peak which is not reproduced, as indicated by the green arrows in Fig. 6. Finally, Fig. 6(f),(l) show results where 2 defects have been moved, one 5 nm towards the QD, the other 5 nm away, and in this case the “final” peak in the simulation has a slightly too large blue shift. It is therefore fair to claim that the random error in the r_i is around ± 5 nm; the systematic error is obviously harder to judge, but the agreement in Fig. 2 of [1], also Fig. 4, would suggest that it is small.

-
- [1] J. Houel *et al.*, Main article.
 - [2] R. J. Warburton *et al.*, Phys. Rev. B **65**, 113303 (2002).
 - [3] B. D. Gerardot *et al.*, Appl. Phys. Lett. **90**, 041101 (2007).
 - [4] R. J. Warburton *et al.*, Phys. Rev. B **58**, 16221-16231 (1998).
 - [5] P. A. Dalgarno *et al.*, Phys. Rev. B **77**, 245311 (2008).

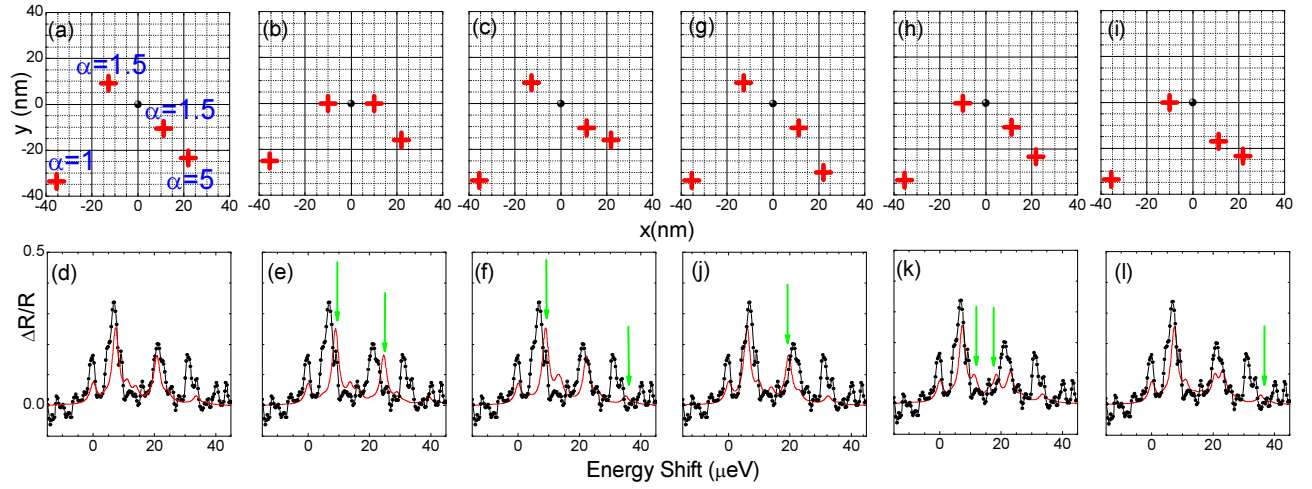


FIG. 6. (a)-(f) 2D representation of the spatial distribution of the above-dot-defects used in the corresponding simulations, (g)-(l). The relative probability α_i for each defect i is stated in (a) and remains the same for all the other configurations. (g)-(l) Line cuts from experiment (black points/lines) at $P = 0.34$ nW and simulation (red lines) at $p = 0.16$. The parameters used in the simulations are those obtained in section I and we take $N = 2,500$ and $\Gamma_L = 1.0 \mu\text{m}$. The distribution in (a) gives the best fit to the data and is used in [1]: all the simulated peaks lie within the linewidth of the corresponding peak in the experimental data. In (b), all the defects are moved 5 nm towards the QD. In (c), the defect with $\alpha = 5$ is moved 5 nm towards the QD. In (d), the defect with $\alpha = 5$ is moved 5 nm away from the QD. In (e), the defect with $x < 0$ and $\alpha = 1.5$ is moved 5 nm towards the QD. Finally, in (f), the defect with $x < 0$ and $\alpha = 1.5$ is moved 5 nm towards the QD while the defect with $x > 0$ and $\alpha = 1.5$ is moved 5 nm away from the QD. In each case, (h)-(l), at least one of the simulated peaks is shifted by at least a linewidth from the peak in the experiment. The particular peaks in question are shown by the green arrows.